RIDGING AND COLOR CHANGES OF ALUMINUM SHEETS DURING PLASTIC STRAINING

MAX-PLANCK PROJECT REPORT

Dierk Raabe, Michael Sachtleber

Max-Planck-Institut für Eisenforschung
Max-Planck-Str. 1
40237 Düsseldorf
Germany

März 2004, Max-Planck-Society
http://www.mpg.de http://www.mpie.de http://edoc.mpg.de/

***KEYWORDS**: electron backscattering diffraction, roughness, aluminum, coating, sheet forming, surface mechanics, surface characterization, colorimetry, roping, ridging, color changes, texture, EBSD, surface strains*

Project References

D. Raabe, M. Sachtleber, H. Weiland, G. Scheele, and Z. Zhao: Acta Materialia 51 (2003) 1539-1560.
„Grain-scale micromechanics of polycrystal surfaces during plastic straining”

D. Raabe, M. Sachtleber, L. F. Vega, and H. Weiland: Advanced Engineering Materials, 4 (2002) p. 859-864.
“Surface Micromechanics of Polymer Coated Aluminium Sheets during Plastic Deformation”

PROJECT ABSTRACT

The project report presents experimental results about surface roughening and color changes of coated (siloxane, soft anodic, epoxy) 6022-T4 aluminum sheets during plastic straining. Experiments are carried out using confocal microscopy and colorimetry. It is found that surface roughening of coated aluminium sheets during plastic deformation is a pronounced function of strain. Different strain regimes and loading modes can lead to different roughening mechanisms. This is indicated by changes in the slope of the roughness-strain curves. The roughening behavior of coated aluminium sheets can substantially differ from that of uncoated sheets of the same substrate material owing to the mechanical properties of the coatings. The coatings which differ in lightness and color values due to their layer thickness and chemical composition can in part undergo substantial changes in these values during straining. Small plastic strains affect in particular changes in color lightness.

INTRODUCTION

Motivation for the work

Structural lightweight materials with functional polymer and metaloxide layers play an increasing role in the transportation, illumination, packaging, food, construction, and design industries. Particular attention must be placed in this context on the growing interest in the *finish first – fabricate later* philosophy. This strategy of modern process engineering means that sheet metal is first coated and subsequently plastically formed to a high quality surface finish. This new method of manufacturing semi-finished parts requires that both, the sheet substrate metal and the coating have excellent surface properties after elastic-plastic loading in terms of the surface roughness, surface patterns, optical appearance, and related functional characteristics.

Plastic straining of coated polycrystalline sheet metals is often accompanied by the gradual development of microstructural defects at the surface as well as in the interface between the metal and the coating. These defects are due to a variety of dynamical mechanisms which are essentially induced by bulk plasticity of the metal substrate. They micromechanically interact with the polymer or oxide coatings and transfer some of the metallic roughness generated during plastic loading through that layer to the surface.

Surface changes created during the plastic co-deformation of coating and substrate metal often entail also a change in color type and color intensity of the polymer and oxide coatings. Such changes are due to the displacements of the pigments and colorants in the polymer. The change in surface roughness also affects optical scattering and, therefore, the reflection of light. More severe surface defects are the formation of orange peel or ridging. These effects exceed in relevance the above mentioned small scale roughening issues since they affect not only the decorative appearance of materials but also their forming limits as

well as the frictional conditions during forming. Altogether these various effects are of importance for understanding and optimizing the visual appearance and the micromechanics of surfaces of formed semi-finished parts [1,2].

In order to optimize and control the final surface structure of formed coated sheets it is important to systemize the observations and extract from them the main microstructural mechanisms. The present work focuses on the description and interpretation of the micromechanics and topography associated with the elastic-plastic co-deformation of polycrystalline aluminum sheets and different layers such as siloxane, soft anodic, and epoxy coatings. Experiments are conducted using in-situ measurements of the surface topography via whitelight confocal microscopy during flat tensile testing and colorimetry analysis during bending.

Theoretical Background

In the context of surface roughness phenomena it is principally useful to differentiate between *intrinsic* and *extrinsic* defects at the surface and in the metal-polymer interface [1,2]. *Intrinsic* surface defects induced by bulk plasticity of the substrate occur in the form of net residual surface displacement fields as a result of microstructure dynamics during plastic straining. Examples are dislocation glide steps, shear bands, orange peel due to hard and soft grains, or mesoscale deformation patterns arising from the co-deformation of clusters of similarly oriented grains [1,2]. As *extrinsic* surface defects we denote all surface changes that occur through the influence of the environment, i.e. by mechanical contact (tools, friction, non-homogeneity of forces and material flow) or by corrosion.

Intrinsic surface and metal-polymer interface defects occur at different spatial scales and can have different microstructural origin, similar to the corresponding hierarchy of bulk de-

fects associated with elastic-plastic loading. Grain-scale micromechanical effects at the sheet surface or respectively metal-polymer interface are essentially determined by orange peel and ridging phenomena. These mechanisms are particularly relevant for the evolution of surface roughness and friction during sheet metal forming, as well as for strain localization and optical appearance at an engineering scale.

Grain-scale surface roughening has been investigated by various groups with respect to the microstructure dependence of wear and with respect to the relation between microstructure and surface patterning. Most recent studies in this field focused on quantitative microstructure experiments with high spatial in-plane resolution. Attention was placed on the dependence of roughening on grain size, strain, and crystallographic texture. Early studies showed that surface roughness increases with the von Mises or respectively through-thickness strain and with the grain size [3-10]. At low strains both dependencies were often found to be linear. Increasing deviations from a linear relation were observed at medium and large strains. For instance Wilson et al. [7] found a non-linear dependence of surface roughness on grain size and strain at large plastic strains.

Deviations from linearity were also found by Mizuno and Mulki [8]. More recent work on brass, however, revealed a linear dependence of surface roughness on both, strain and grain size up to large strains of 0.8 (logarithmic strain) [10]. Also, a close connection was observed between grain-scale surface roughening and crystallographic texture. More precisely, the microtexture, the misorientation distribution, the two point correlation function, the global texture, as well as individual crystalline shear and reorientation rates were related to grain-scale roughening [1,7,11-21]. Due to these studies local texture analysis plays an increasing role for surface micromechanics [e.g. 1,2,17]. An important consequence of the close relationship between texture and roughening is that surface micromechanics must be regarded as a tensorial and not a scalar problem, i.e. the deformation *mode* has an influence on surface roughness [22]. Vice versa surface topology was observed to have a significant influence on the forming limits of sheet material. For instance Yamaguchi et al. [22] showed that an increase in the forming limits of polycrystalline sheet metals could be achieved by

removing surface roughness. The experiments were conducted on balanced biaxial stretching of aluminum sheets and foils. This observation also underlines the close correlation of strain localization, strain hardening, and surface roughness. Similar observations were made by Jain et al. [9] who investigated the relation between strain hardening, grain size, and surface roughening with respect to biaxial tensile limit strains of aluminum.

An important result of this work was that the use of the average grain thickness as a measure of the grain size provided a good means for predicting surface roughness during straining. Mahmudi and Mehdizadeh [10] investigated surface roughening during plastic straining in uniaxial and equi-biaxial stretching experiments using 70-30 brass sheets. Their study showed for a wide range of parameters a good correlation between grain size and surface roughness. It was found that the roughness increment was proportional to the applied strain and to the grain size of the sheets. The authors found for all investigated materials that roughness was more pronounced in transverse direction (referring to the coordinate system imposed by rolling) than in longitudinal direction. The authors concluded that the non-uniformity of the grain structure, together with the inhomogeneities present in the material, acted as main sources of surface roughening. Lee et al. [14] investigated the development of grain scale roughening (orange peel) in an aluminum 6022-T4 sheet by using interference microscopy and electron back scattering diffraction (EBSD) experiments. No clear relationship was identified between orange peel and the orientations of surface grains. Brass-oriented grains, {011}<21$\underline{1}$> (φ_1=35°, ϕ=45°, φ_2=0°), tended to be located in the high spots or peaks of the surface of the deformed specimen. Surface height gradients predicted from allowing the surface grains to shear in relaxed constraints mode were weakly correlated with the experimental surface height gradient. Wittridge and Knutsen [16] investigated the evolution of grain-scale surface roughness during uniaxial tensile deformation, placing particular attention on the development of parallel ridges and valleys in aluminum sheets. Their analysis was based on using polarized light microscopy as well as bulk and microtexture measurements. The authors interpreted the results in terms of in-plane spatial differences in texture at the sheet surface. They found that colonies of the R texture component, which were embedded in a matrix with predominant Cube orientation, produced differential strain-

ing, which entailed strain localization and a corrugated profile. This observation confirmed the fact that grain-scale roughening first produces microscopic strain localization at the sheet surface in the incipient stages of plastic straining and eventually macroscopic through-thickness strain localization. In accordance with earlier work the authors suggested that ridging phenomena could be attributed to the inhomogeneity of the microtexture.

Another recent study was published by Baczynski et al. [17] about roping phenomena in an aluminum 6111 alloy. In this work the authors investigated roping and non-roping materials obtained from two different processing routes. In contrast to earlier work their study showed that both ridges and valleys on the upper and lower surfaces were irregularly distributed in the rolling direction, i.e. they were not in synchrony. Ribbed profiles as well as corrugations were only rarely observed. By using electron back scattering diffraction (EBSD) experiments the authors demonstrated that the spatial distribution of Goss oriented grains were mainly responsible for the roping behavior in the investigated alloy. Furthermore, the authors found that the work hardening rates of roping and non-roping specimens were similar. The anisotropy of fracture elongations in the sheet plane was found to be significantly larger in the roping than in the non-roping material. This observation was interpreted in terms of the strong anisotropy of the Goss texture component in the roping material. Huh and Engler [18] investigated the effects of intermediate annealing on texture and ridging of a 17%Cr ferritic stainless steel. They observed that sheets with weaker through-thickness texture gradients as well as enhanced recrystallization textures were less prone to show pronounced ridging. Similar observations were made by Salsgiver et al. [19]. Engler et al. [20,21] also presented two articles on the correlation of ridging and texture in Al-Mg-Si (6xxx) sheets revealing in particular a clear correlation between the orientation density of Cube and the ridging height. Raabe et al. [1] recently submitted a study about the roughening of a set of AA6022 aluminium sheets in which they established a clear relationship between plastic microstrains, surface topography, precipitations, and the topological clustering of certain texture components, for instance Cube.

EXPERIMENTAL PROCEDURE

In-situ tensile deformation set-up

In order to characterize free surface roughening of coated aluminum sheets, in-situ tensile tests were conducted on a set of Al-Mg-Si aluminum sheet samples (AA6022, T4 condition) with identical chemical composition and substrate microstructure but different coatings. For the present study we use soft anodic, siloxane, and epoxy coatings. The various coatings were chosen because they differ in their mechanical properties. While the coatings revealed slight differences in thickness the thickness of the substrate metal was held constant in all cases (1.0mm).

Since it is known that the intensity of surface ridging of aluminum is often larger when the samples are strained in transverse direction to the former rolling direction all tensile tests were conducted parallel to the transverse direction [1,2].

A small tensile machine was mounted on a lateral x-y stage parallel to the plane set up by the transverse and rolling direction of the coated aluminium sheets. The device was placed under a confocal white-light microscope. The cross heads of the tensile substage moved in opposite directions in order to minimize the relative motion of the scanned area which was kept close to the center of the tensile specimen. Each dogbone shaped tensile specimen had a nominal thickness, width, and length of 1mm × 5mm × 50 mm, respectively. The loading speed amounted to 10µm/s and the maximum load was 1.7 kN.

Deformation was carried out in a series of subsequent steps up to 17% accumulated plastic straining in the transverse direction of the samples (engineering plastic tensile strain). After each deformation step the load was kept constant. The surface topography of the elongated specimens was measured during these breaks by using the confocal microscope providing a

three dimensional surface roughness mapping. An area of 0.7 x 0.7 mm was examined on identical surface regions, allowing us a one-to-one comparison of the evolution of the same sample area at subsequent stages during straining. Prior to deformation, each initial sample surface roughness was recorded. In order to include surface defects which were inherited from preceding rolling the samples were not polished before the confocal analysis.

In-situ topography characterization

The confocal microscope works on the basis of a point distance measurement using a depth discrimination method in reflection mode. In a first focusing step light which is emitted from a point source is imaged into the object focal plane of a microscope objective. An in-focus specimen location results in a maximum flux of the reflected light through a detector pinhole (second focusing), whereas light from defocused object regions is partly suppressed. Therefore, the detector signal as limited by the pinhole size is reduced drastically when defocusing the specimen. For the current study this principal design was improved for fast 3D measurements by use of a spinning multiple pinhole mast (Nipkow disk) in an intermediate image plane of a microscope. The Nipkow-disk consists of an array of pinholes arranged in a spiral shape. The disk which is operated in a spinning mode is illuminated by a plane wave and acts as a scanning multiple point light source which is imaged into the object focal plane of the microscope objective. After the reflection of light each illuminating Nipkow pinhole acts as its own detector pinhole. Combined with fast CCD image processing the rotating Nipkow disk affects the in-plane-scan of the object field in video-real-time. Therefore, only the additional out-of-plane scan is required for 3D acquisition. The Nipkow-disk expands the effect of depth discrimination to the area of the microscope object field, which allows optical sectioning like in computer tomography.

Colorimetry analysis during bending

The quantification of color changes occurring during forming of coated sheets is an essential ingredient in developing robust finish first – fabricate later philosophies particularly for automotive applications. In order to analyze such color changes during plastic deformation we conducted bending tests with subsequent color analysis on the coated samples described above. Similar to the flat tensile samples the straining direction (=bending direction) coincided with the transverse direction as described above. Deformation was performed using a guided bend test set-up (Fig.1). The samples were clamped in a vise and manually bent over a fixed cylinder with a radius of 7mm without lubrication. Bending was carried out in two subsequent bending steps of a 30° angle each. The bending angle was controlled by a protractor in the unload state after each deformation step. Prior to each bending step the surface color was recorded using a colorimetric method.

Colorimetry comprises methods for the identification of colors and differences among colors with the aim to define and quantify perceptual color fidelity metric systems. In the first place color is a physical property of a material that depends on the spectral distribution of incident light and on the light which is reflected in the visible range of the electromagnetic spectrum. A second important aspect of color perception lies in the fact that it is necessary to quantify how accurate the reproduction of a color is to the original when viewed by a *human observer*. This means that colorimetric measures for color discrimination are determined by a lot of quite different factors, such as the cone sensitivity of the eye, the ambient illumination, and the spatial pattern of the targets. When using the various metrics it must be considered that the effects of some of these factors on color sensitivity are better understood than others. Most of the current means for quantifying visual perception of colors have been introduced by the International Committee of Illumination (CIE). The CIELAB metrics aim at measuring color differences among uniform color targets. One of the most widely used perceptual color fidelity metric is the CIE L-a-b standard color space specification. The

three parameters L, a, and b are defined in the three dimensional *CIELAB color space* classified by the CIE in 1976 (Fig. 2). In order to measure perceptual difference between two colors using this metric, the spectral power distribution of the two colors are first converted to XYZ representations, which reflect within a linear transformation the spectral power sensitivities of the three cones on the human retina. Then, the XYZ values are transformed into an L-a-b space, in which equal distance is supposed to correspond to equal perceptual difference. This means that the L-a-b space can be understood as a *perceptually uniform* space. Then, the perceptual difference between the two targets can be calculated by taking the Euclidean distance of the two in this L-a-b space. In the L-a-b space the L-axis is the lightness and extends from 0 (black) to 100 (white). The greater the L number is, the brighter the color would be; conversely, the smaller the number is, the darker the color would be. The color components a and b are indices which denote the degree of the three primary colors. Larger values of a and b correspond to a more red and more yellow color, respectively. The smaller these two numbers are the more green and the more blue the color, respectively. Samples with a=b=0 are achromatic, i.e. the L-axis represents the achromatic gray scale axis ranging from black to white. Deviations of the CIE L-a-b- parameters measured by a colorimeter are effectively used for quality control as a standard procedure in the automotive industry. In this study a standard L-a-b colorimeter is used to quantify changes in color which the tested surfaces undergo during plastic bending.

EXPERIMENTAL RESULTS AND DISCUSSION

Figs. 3 to 6 show the evolution of surface roughening as a function of plastic strain during flat tensile testing of the uncoated substrate material (Fig. 3) and of the different coated samples (Figs. 4-6). The topography maps were assembled using white-light confocal microscopy as outlined above. The color code represents the height of each surface point in

reference to an absolute minimum at 0.0 µm. The presented topography maps have been form corrected for macroscopic undulations. All sketches taken subsequently from the samples for topography measurements cover a constant area fraction. This means that a slight shift occurs during each test from sketch to sketch between the sample coordinate system which is gradually elongated in the transverse direction and the observed topography.

The surface *patterns* of the uncoated (Fig. 3), of the anodic coated (Fig. 4), and of the siloxane coated (Fig. 5) samples reveal a similar evolution. Below 5% engineering plastic transverse strains the surfaces are characterized by weak initial elongated roughness patterns aligned parallel to the former rolling direction. These patterns do not have an intrinsic microstructural background but are inherited from the preceding cold rolling process. At transverse strains above 5% all three samples reveal a transition regime. The elongated roughness patterns gradually change into a non-directional equiaxed surface topology. This transition process ends after 17% transverse strain with the complete loss of the inherited elongated surface structures. The intrinsic surface structures generated during this regime can be interpreted in terms of orange peel effects. Such phenomena describe mechanisms where crystals at the surface undergo individual out-of-plane displacements (negative or positive) which roughly map the grain shape or grain-cluster shape of the material. Similar observations were described in [1] and in [17].

The surface patterns of the epoxy coated sample show a completely different behavior (Fig. 6). Due to the coating process and the mechanical properties of the epoxy, the inherited elongated surface pattern of the substrate metal was not preserved during coating. It was completely covered by the epoxy layer entailing a new surface pattern with a longer wavelength prior to straining. This means that the epoxy coated sample does not show any linear surface patterns at the initial state. The topology evolution of the epoxy coated material is dominated by non-directional equiaxed surface patterns.

The topography maps of the uncoated samples (Fig. 3) and of the siloxane coated samples (Fig. 5) reveal very similar roughening behavior during plastic straining. The soft anodic

coated (Fig. 4) and the epoxy coated samples (Fig. 6) show a slightly stronger roughening and a higher initial surface topography. At strains of about 17% elongation in transverse direction all topography maps – except the epoxy coated specimen – show similar surface roughness in terms of pattern and height distribution.

The intensity of surface roughening can be discussed in terms of the three-dimensional surface parameter S_a as a function of the plastic strain. The surface parameter S_a quantifies the mean absolute deviation from the mean displacement parallel to the sheet normal direction,

$$S_a = \frac{1}{NM} \sum_{RD=1}^{N} \sum_{TD=1}^{M} \left| z_{RD,TD} \right| \qquad (1)$$

where N and M are the numbers of values in the two perpendicular in-plane axis directions (rolling direction and transverse direction), and $z_{RD,TD}$ are the absolute values of the residual plastic displacements perpendicular to the plane.

Figs. 7 and 8 show the development of the surface parameter S_a as a function of the engineering strain. The initial surface roughness spreads from 0.3 µm for the siloxane coated and for the uncoated material up to 0.55 µm for the epoxy coating and for the soft anodic coating. Besides the differences in the initial state the siloxane coating, the soft anodic coating, and the uncoated material end up with a surface roughness of about 1.2 µm. With a value of about 1.5 µm the epoxy coated sample reveals a more pronounced roughness in the high-strain regime (Fig. 7c).

A more detailed analysis of the topography evolution can be given after Gaussian filtering. This type of filter separates surface effects into short wavelength effects (*roughness*) and large wavelength effects (*waviness*) by using a wavelength threshold. The threshold level was adapted to the microstructural scaling of the material. Short range effects typically exist of a range of only some grains and long range surface effects have a range significantly above the grain size. Since the average grain size of the material is 30 µm in diameter we used a threshold of 250µm in the current analysis.

Figs. 7 and 8b show that all samples reveal similar tendencies in their short wavelength effects (roughness) in terms of the slope of the roughness-strain curves. Different behavior occurs in the long wavelength behavior (Fig. 8c). The epoxy coated material reveals the strongest waviness and at the same time the smoothest roughness evolution. The largest roughness is observed for the soft anodic coated material (Figs. 7b, 8b). In clear contrast to the other specimens the epoxy coated material is essentially dominated by its pronounced waviness (Fig. 8c). The siloxane coating reveals a behavior during plastic straining which is basically different from that of the epoxy coated material. Due to its soft mechanical properties the siloxane coating does not level out the inherited extrinsic roughness of the substrate sheet. During plastic straining it follows essentially the roughness evolution prescribed by the substrate material. Besides the details of the patterns discussed above Fig. 7 and 8 also substantiate that the qualitative analysis of the topography patterns (Fig. 3-6) made by eye rating is matched very well by the quantitative curves of the surface parameter S_a.

Fig. 9 shows the change in color and brightness of an identical set of coated samples during bending deformation as measured by colorimetry. The bending direction was parallel to the transverse direction of the sheet. Deformation was conducted in two subsequent bending steps of 30° bending angle each. The data demonstrate that the samples reveal a constant L-value in the range of 50 to 65 during bending. It is worth to note that only the siloxane coated material shows a lightness level much below that of the other specimens. It reveals a slight increase in the L-value from 15 to 25 during bending.

The siloxane und epoxy coated sheets reveal a constant a-value during bending close to zero which corresponds to a gray-scale color perception. In contrast, the uncoated sheet, the material with soft anodic coating, and the acrylic powder coated specimen has a negative initial a-value. For all threes samples the a parameters increase during the first bending step and remain essentially constant at larger bending angles. The uncoated material shows a drastic increase in the a-value from -37 to +20, i.e. it undergoes a change from blue to red.

All samples except the siloxane coated specimen show similar initial b-color-values in the range of +25 to +35. The siloxane coating lies in the range of zero and does not change its color during bending. The rest of the tested samples reveal a decreasing b-value with the first bending step. Their color appearances remain unchanged during the second bending step. The uncoated material shows opposite behavior, i.e. it is constant during the first bending step, but it reveals a drastic change in color at larger bending angles.

CONCLUSIONS

We presented experimental results about surface roughening phenomena and corresponding color changes of coated aluminum sheets during plastic straining. Experiments were conducted using in-situ measurements of the surface topography via whitelight confocal microscopy during flat tensile testing and colorimetry analysis during bending. The study concentrated on the description and interpretation of the observed micromechanics, topography, and colorimetry associated with the elastic-plastic co-deformation of the polycrystalline aluminum sheets and their different coatings. The main results are:

- The micromechanical behavior and surface roughness of aluminium sheets with polymer or inorganic coatings during plastic co-deformation must be carefully investigated as a function of strain. Different strain regimes can reveal different roughening mechanisms.
- The strain-induced roughening behavior of coated aluminium sheets can substantially differ from that of uncoated sheets of the same substrate material owing to the mechanical properties of the coatings.
- Some coatings such as siloxane level out the inherited sheet roughness to a certain extent and smoothen the co-deformed surface. The epoxy coating was an example of coatings which increase the surface roughness of the substrate metal in terms of absolute height and revealed a completely different surface pattern when compared to the uncoated substrate material.
- Coatings differ in lightness and color values due to their layer thickness and chemical composition. Plastic deformation of coated samples leads in part to substantial color changes. Small plastic strains affect in particular changes in lightness.

REPORT REFERENCES

1. Raabe, D., Sachtleber, M., Weiland, H., Scheele, G., and Zhao, Z.: Acta Materialia 2003, **51,** page 1539.
2. Raabe, D., Sachtleber, M., Vega, L. F., and Weiland, H.: Advanced Engineering Materials, 2002, **4**, page 859.
3. Mietzner, K., *Stahl und Eisen*, 1961, **81**, page 950.
4. Kienzle, O. and Mietzner, K., *Atlas Umgeformter Metallischer Oberflächen.* Springer-Verlag, Berlin, Germany, 1967.
5. Osakada, K. and Oyane, M., *Bull. J.S.M.E.*, 1971, **14**, page 171.
6. Fukuda, M., Yamaguchi, K., Takakura, N. and Sakano, Y., *J. Japan Soc. Technol. Plasticity*, 1974, **15**. page 994.
7. Wilson, D. V., Roberts, W. T. and Rodrigues, P. M. B., *Metall. Trans.*, 1981, **12A**, page 1603.
8. Mizuno, T. and Mulki, H., *Wear*, 1996, **198**, page 176.
9. Jain, M., Lloyd, D. J. and MacEwen, S. R., *Int. J. Mech. Sci.*, 1996, **38**, page 219.
10. Mahmudi, R. and Mehdizadeh, M., *J. Mater. Proc. Techn.*, 1998, **80–81**, page 707.
11. Takechi, H., Kato, H., Sunami, T. and Nakayama,T., *Trans J.I.M*, 1967, **8**, page 233.
12. Chao, H.-C., *Trans. ASM*, 1967, **60**, page 37.
13. Becker, R., *Acta mater.*, 1998, **46**, page 1385.
14. Lee, P.S., Piehler, H. R., Adams, B. L., Jarvis, G., Hampel, H. and Rollett, A.D., *J. Mater. Proc. Techn.* 1998, **80–81**, page 315.
15. Bethke, K., Hölscher, M. and Lücke, K., *Mater. Sci. Forum*, 1994, **157**, page 1137.
16. Wittridge, N. J. and Knutsen, R. D., *Mat. Sc. Engin.* 1999, **A269**, page 205.
17. Baczynski, G. J., Guzzo, R. Ball, M. D. and Lloyd, D. J., *Acta mater.* 2000, **48**, page 3361.
18. Huh, M.-Y. and Engler, O., *Mat. Sc. Engin.* 2001, **A308**, page 74.
19. Salsgiver, J. A., Larsen, J. M. and Borneman, P. R., in *Proc. Int. Conf. Recrystallisation '90*, ed. T.Chandra, The Minerals, Metals and Materials Society, TMS, 1990, page 849.
20. Engler, O. and Brünger, E., *Mater. Sc. Forum* 2002, **396-402**, page 345.
21. Engler, O. and Hirsch, J., *Mat. Sc. Engin.* 2002, **A336**, page 249.
22. Yamaguchi, K., Takakura, N. and Imatani, S., *J. Mater. Proc. Techn.* 1995, **48**, page 27.

FIGURES

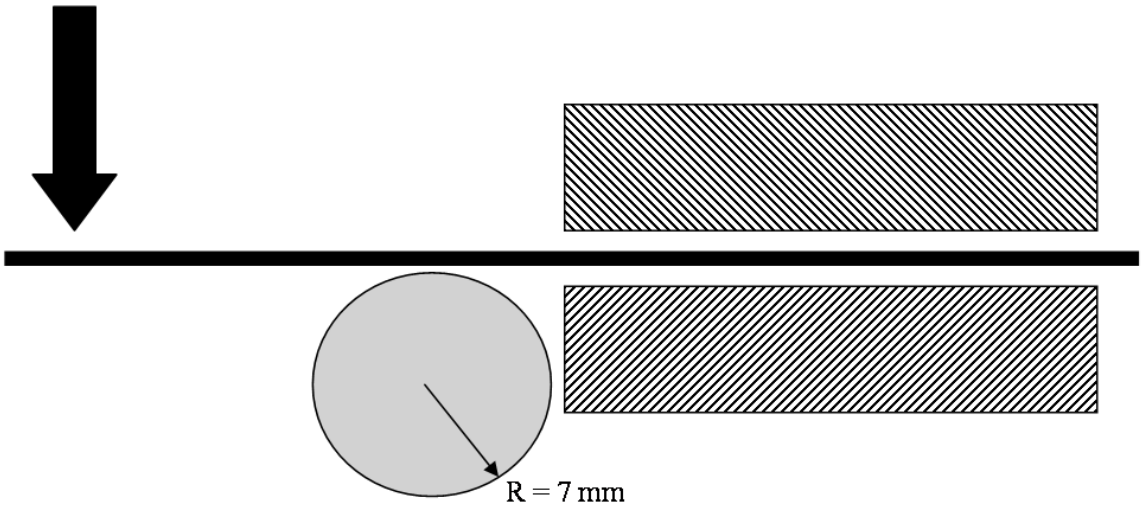

Fig. 1 Guided bend test set-up

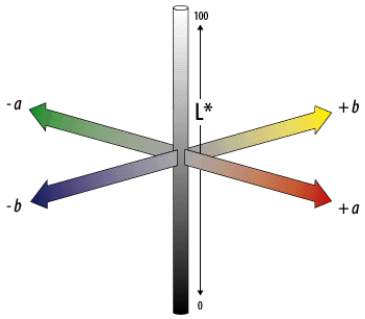

Fig. 2 The L-a-b- standard metric as introduced by the International Committee of Illumination (CIE).

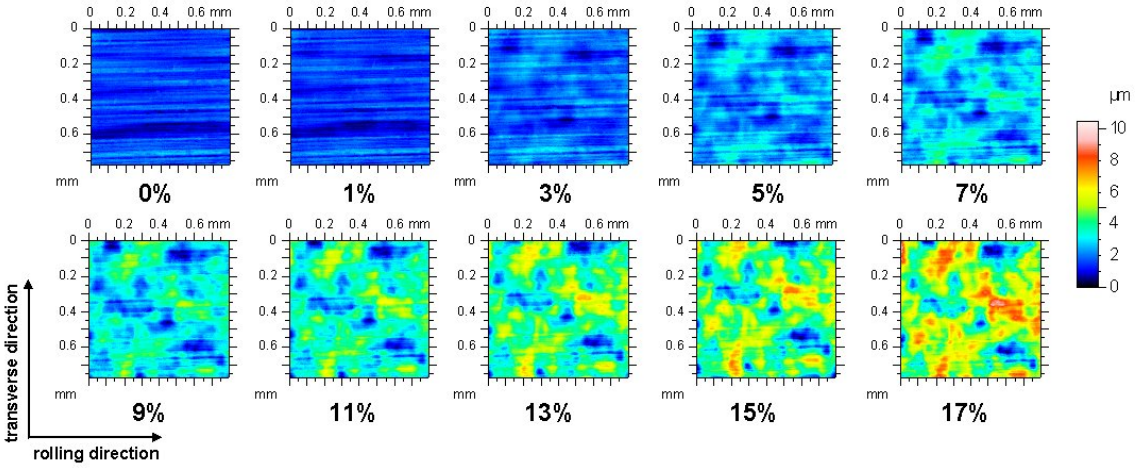

Fig. 3 Development of surface topography of the uncoated aluminium sample during subsequent plastic straining in transverse direction (flat tensile test). The material was an Al-Mg-Si aluminum alloy in T4 condition.

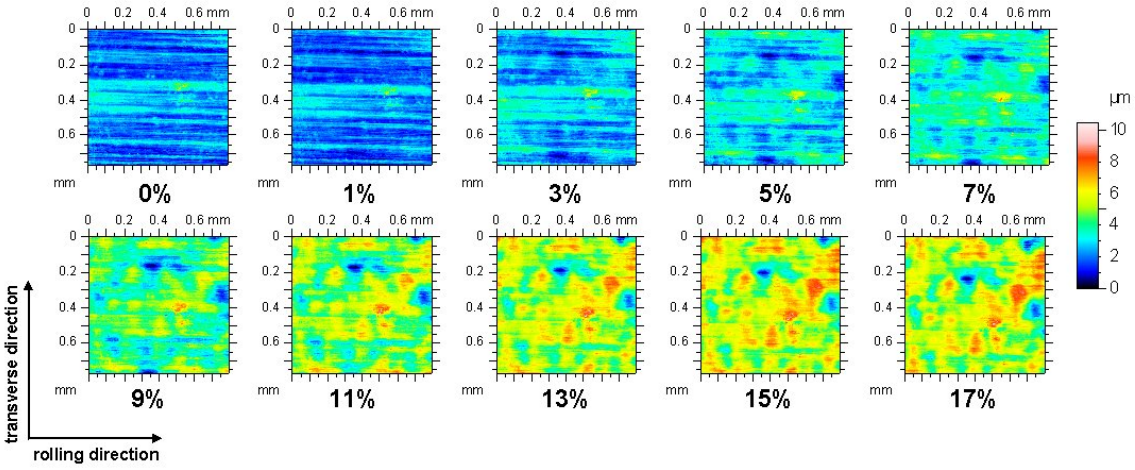

Fig. 4 Development of surface topography of the soft anodic coated sample during subsequent plastic straining in transverse direction (flat tensile test). Substrate material was an Al-Mg-Si aluminum alloy (AA6022) in T4 condition.

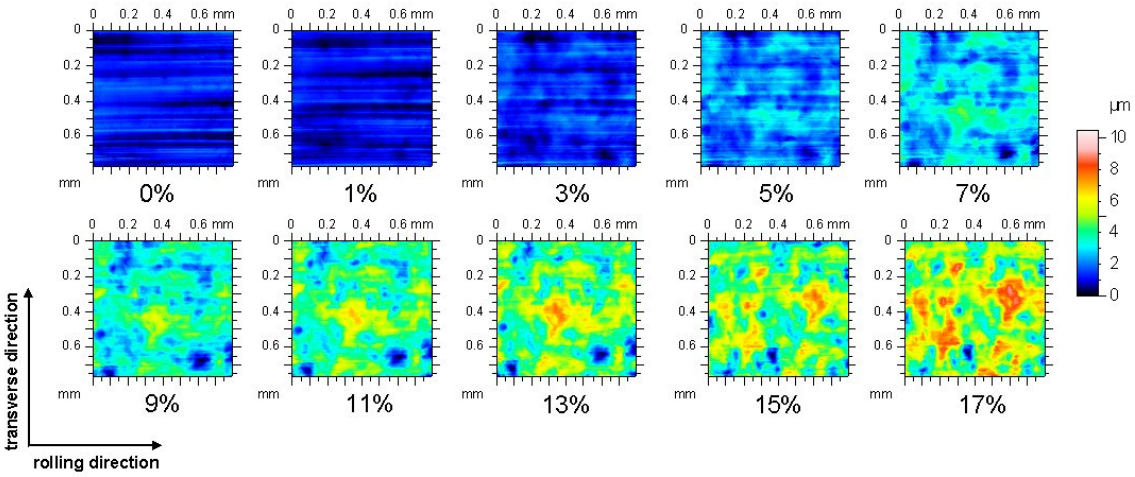

Fig. 5 Development of surface topography of the siloxane coated sample during subsequent plastic straining in transverse direction (flat tensile test). Substrate material was an Al-Mg-Si aluminum alloy (AA6022) in T4 condition.

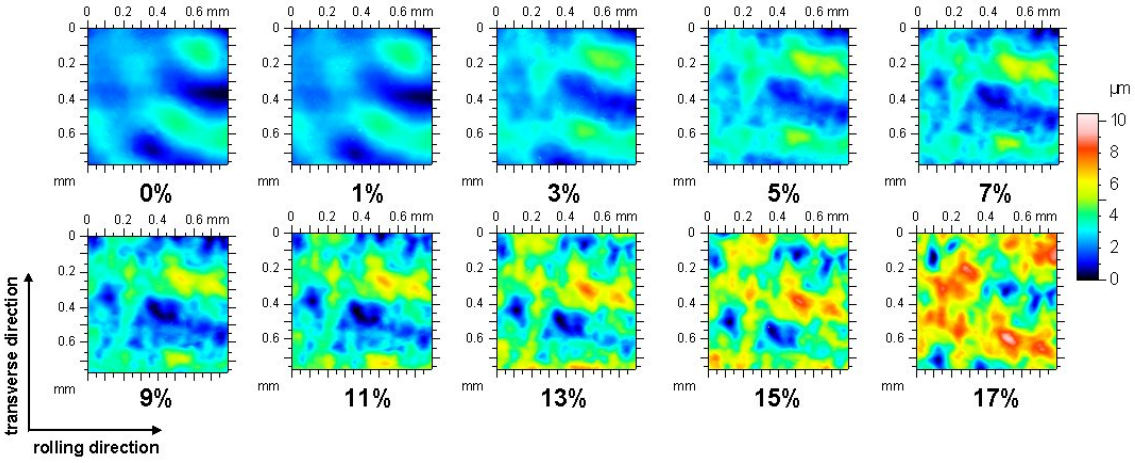

Fig. 6 Development of surface topography of the epoxy coated sample during subsequent plastic straining in transverse direction (flat tensile test). Substrate material was an Al-Mg-Si aluminum alloy (AA6022) in T4 condition.

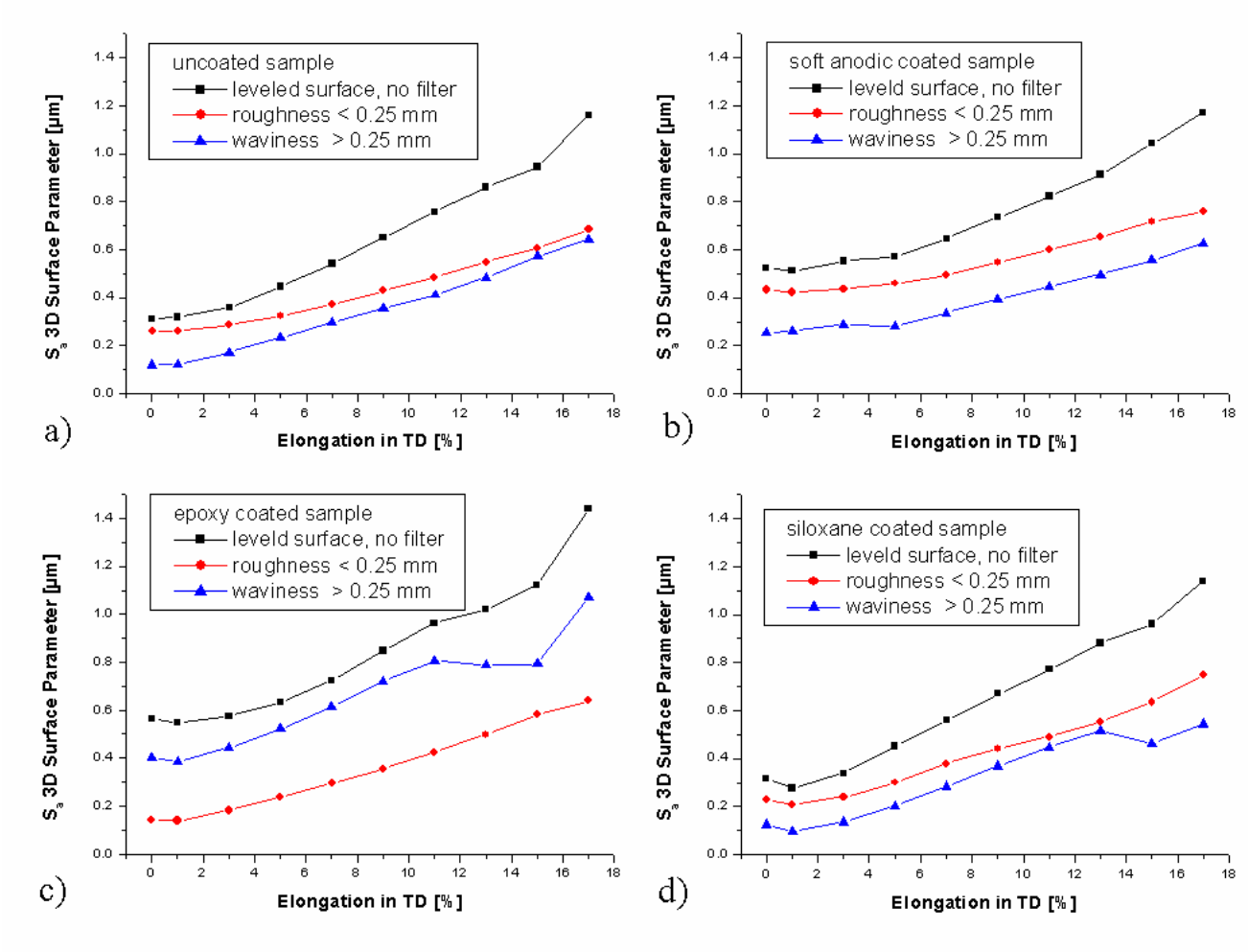

Fig. 7 Evolution of surface roughness as a function of plastic strain for coated and uncoated samples during flat tensile testing in transverse direction. Gaussian filtering separates long-range wavelength effects from short-range roughness effects. Separation criterion is a wavelength threshold of 0.25mm.

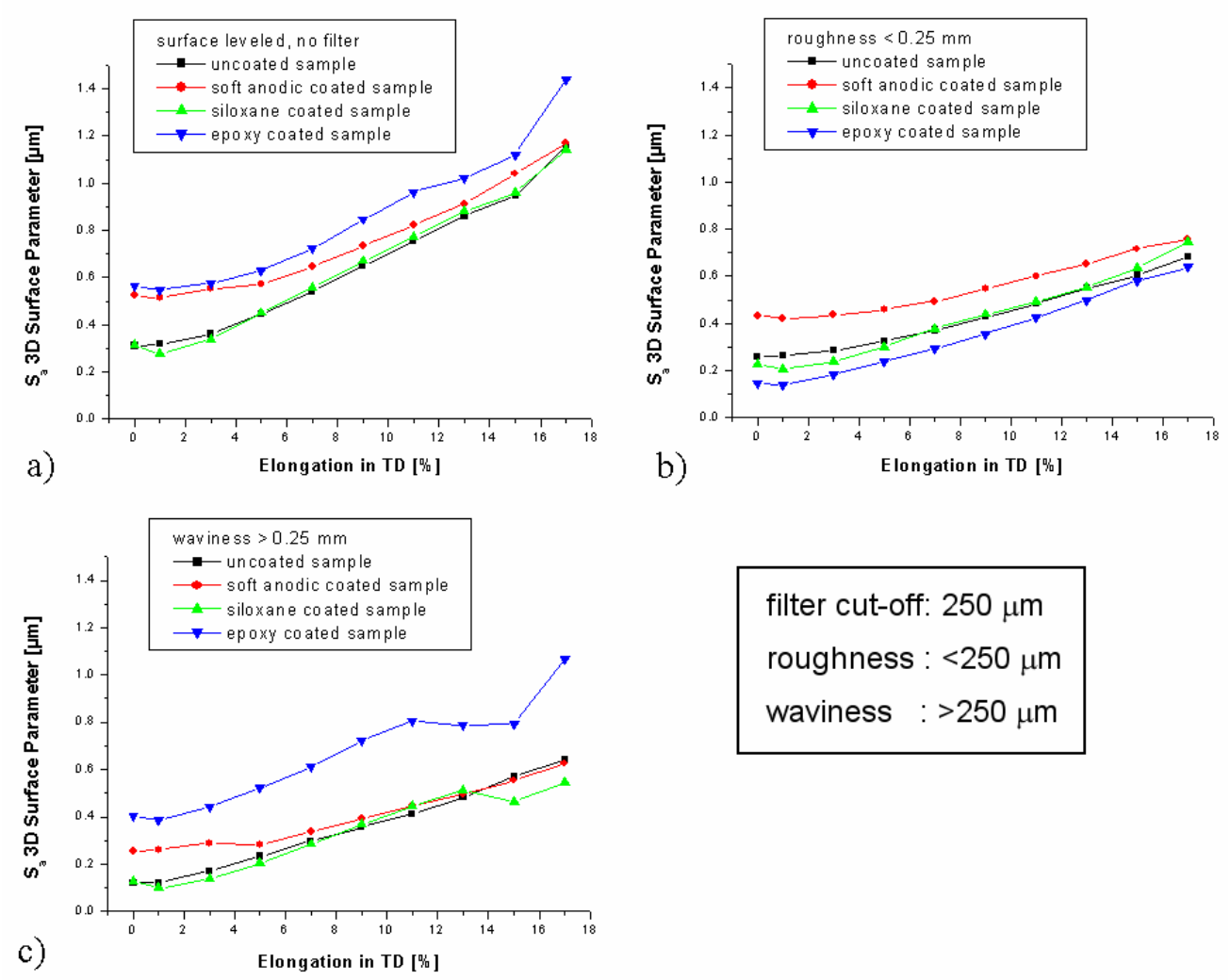

Fig. 8 Overview of the surface roughness as a function of plastic strain for coated and uncoated samples during flat tensile testing in transverse direction. Gaussian filtering separates long-range wavelength effects from short-range roughness effects. Separation criterion is a wavelength threshold of 0.25mm.

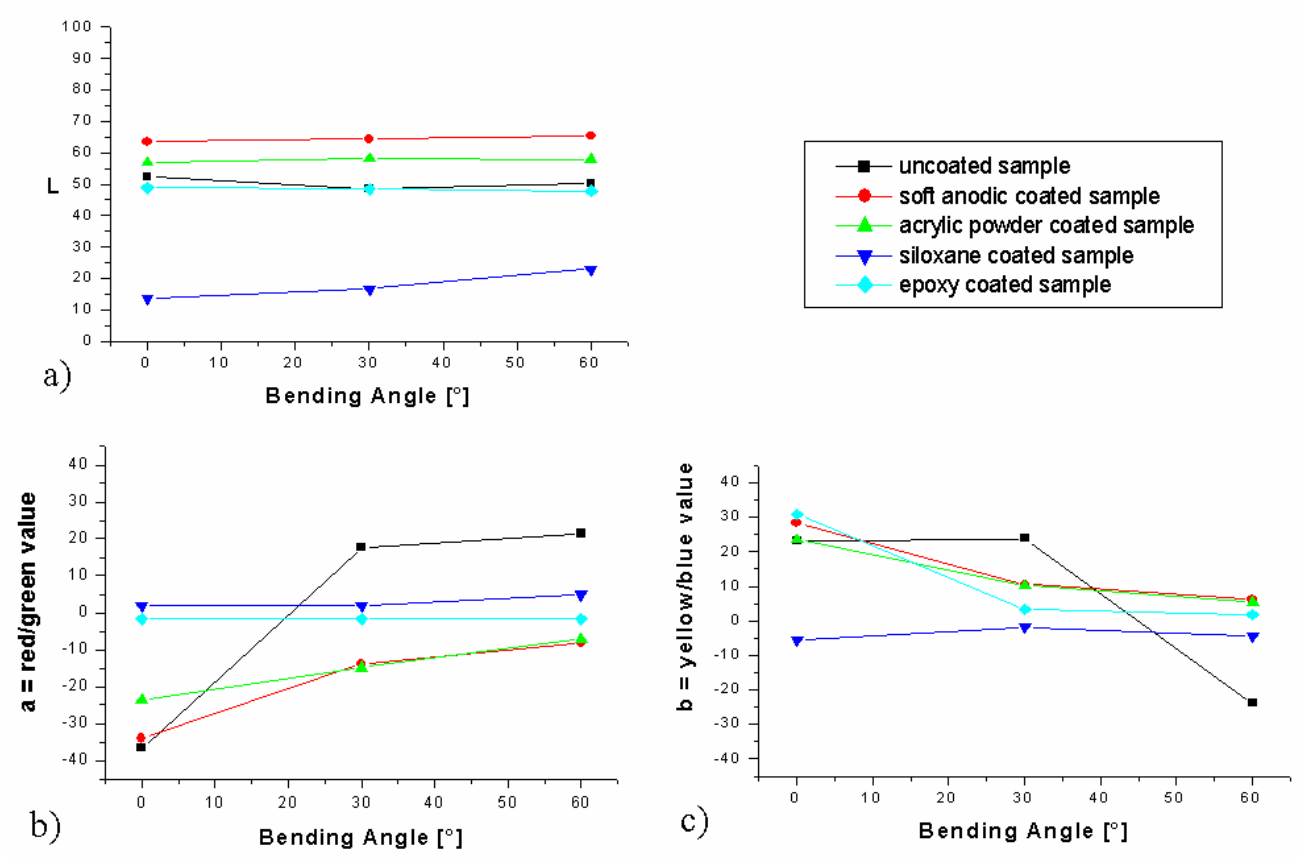

Fig. 9 Colorimetry of coated and uncoated samples. Deviations are quantified in terms of L, a, and b parameters defined by the three dimensional color solid during bending deformation carried out in two subsequent bending steps of 30° each (see also Fig. 1).